PCCP

ROYAL SOCIETY OF CHEMISTRY

PAPER

View Article Online
View Journal

Check for updates

Cite this: DOI: 10.1039/d2cp01649d

Anion photoelectron spectroscopy and density functional theory study of $TM_2Si_n^-$ (TM = V, Cr; *n* = 14–20) clusters†

Kai Wang,‡[a] Guang-Jia Yin,‡[a] Ze-Zhao Jia,[a] Lin Miao,[a] Ramiro Moro,[a] Bernd von Issendorff[b] and Lei Ma *[a]

Received 9th April 2022,
Accepted 17th July 2022

DOI: 10.1039/d2cp01649d

rsc.li/pccp

We investigated the structural evolution and electronic properties of medium-sized silicon cluster anions doped with two transition metal atoms, $TM_2Si_n^-$ (TM = V, Cr; *n* = 14–20), by using mass-selective anion photoelectron spectroscopy combined with density functional theory (DFT) calculations. Putative ground state structures of these clusters were obtained by using a genetic algorithm coupled with the DFT calculations. It was found that the two TM atoms tend to form a TM–TM bond, which – except for $V_2Si_{19}^-$ – is shorter than the nearest neighbour distance in the crystalline state of the respective metals. The $V_2Si_n^-$ clusters with *n* = 14 to 17 exhibit structures based on a silicon hexagonal antiprism, while the larger ones exhibit more fullerene-like cage structures. $Cr_2Si_n^-$ clusters follow the same trend, although with a silicon hexagonal prism structure for *n* = 14 and 15, and the transition to fullerene-like structures occurring at *n* = 17. Among these clusters, $TM_2Si_{18}^-$ have the largest average binding energy and second order differences in energy, therefore the highest relative stability. All of the clusters possess total magnetic moment of 1 μB, but with very different contributions from the doped TM atoms. Especially in the Cr doped clusters there is a tendency towards an anitiferromagnetic arrangement of the magnetic moments of the two Cr atoms.

Introduction

Silicon (Si) clusters doped with transition metal (TM) atoms have been intensively studied experimentally[1–18] and theoretically[19–33] over the past decades due to their unique structural features and potential technical applications in nanomaterials and semiconductors. In particular, vanadium (V) and chromium (Cr) doped Si clusters have attracted much attention as V–Si alloy nanoparticles can be potentially utilized for non-volatile memory devices,[34] and as Cr–Si alloy has been widely applied in making thin film resistors and sensors.[35–37] More recently, a promising catalytic performance of cage-like silicon clusters doped with one V atom, VSi_{12-15}, with respect to carbon dioxide hydrogenation was predicted.[38] Clusters doped by V or Cr dimers have also already been studied theoretically. For example, the stability and magnetic properties of small neutral silicon clusters doped with two chromium atoms Cr_2Si_n (n = 1–8) have been studied by first-principle calculations.[39] Likewise, the geometric structures, magnetic properties and stabilities of neutral V_2Si_{18} and Cr_2Si_{18} clusters have been examined by theoretical investigations.[31]

Different experimental methods have been applied to study V- and Cr-doped Si clusters.[18,40–44] With respect to studies of multiply doped clusters, anion photoelectron spectra (PES) measurements were conducted on $V_{1-2}Si_{3-6}^-$,[8] $V_{1-3}Si_{12}^-$,[12] $V_3Si_{3-14}^-$,[45] and $Cr_nSi_{15-n}^-$ (n = 1–3).[46] Among these clusters, several were found to have peculiar structures and physical properties. $V_2Si_{12}^-$, *e.g.*, adopts a capped hexagonal antiprism structure with a doublet spin state; $V_3Si_{12}^-$ exhibits a bicapped hexagonal antiprism wheel-like structure with a total spin magnetic moment of $4\mu_B$;[12] $Cr_3Si_{12}^-$ has a D_{6d} symmetric wheel structure with a large magnetic moment of $7\mu_B$.[46]

Doping one or more TM atoms into silicon clusters obviously can lead to rather special geometrical structures and physical properties. Therefore, it is attractive to extend the investigation of Si clusters doped with more than one TM atom to larger sizes than studied before; comparing different TM can additionally yield information about the influence of the nature of the TM. Here, we present a study on the

---

[a] *Tianjin International Center for Nanoparticles and Nanosystems, Tianjin University, 92 Weijin Road, Nankai District, Tianjin 300072, China. E-mail: lei.ma@tju.edu.cn*

[b] *Fakultät für Physik, Universität Freiburg, H. Herderstr. 3, D-79104 Freiburg, Germany*

† Electronic supplementary information (ESI) available: See supplementary material for more isomers and their photoelectron spectra; the testing of different functionals; the optimized Cartesian coordinates of the low-lying isomers. See DOI: **https://doi.org/10.1039/d2cp01649d**

‡ K. Wang and G.-J. Yin contributed equally to this work.

structures, electronic and magnetic properties of $TM_2Si_n^-$ (TM = V, Cr; n = 14–20) employing a combination of anion PES experiments and DFT calculations.

Experimental method

The method of cluster synthesis and PES measurement has been described in detail in previous works.[9,18,47,48] In brief, the experiments were performed with a magnetic-bottle PES apparatus equipped with a magnetron sputtering gas aggregation cluster source. The TM–Si (TM = V, Cr) clusters anions were generated in a liquid nitrogen cooled tube filled with a mixture of helium and argon (roughly 3 : 1) with a total pressure of about 0.5 mbar. After production the clusters were guided into a cryogenic radio-frequency 12-pole ion trap cooled to about 80 K. In the trap, the clusters were thermalized by collisions with helium buffer gas with a pressure of about 10^{-3} mbar. They were then inserted into a high-resolution, double reflectron time-of-flight mass spectrometer. Here the clusters were size-selected by a multi-wire mass gate with a resolution of about $m/\Delta m = 2000$. The selected clusters were then irritated by a 248 nm KrF laser in the interaction region of a magnetic bottle-type time-of-flight photoelectron spectrometer. The photoelectron spectra were averaged over typically 30 000 laser shots at a repetition rate of 100 Hz. The spectrometer was calibrated using the measured PES of Pt anion, leading to an error of measured binding energies of less than 30 meV.

Theoretical method

In order to obtain the ground-state structures of the clusters, a global search was performed using our homemade genetic algorithm[18] and the ORCA program with the BP86 functional[49,50] and the def2-SVP basis set for energy calculations.[51–54] In order to ensure a high probability to locate the global minimum on the potential energy surface, more than 3000 configurations were generated for each cluster size. Of these 10–30 lowest-energy isomers were further optimized employing the def2-TZVP[51,52] and the diffuse def2-TZVPD basis set.[51,52,55] Vibration analyses show that the structures have no imaginary frequencies. Zero-point-energy (ZPE) corrections were included for the relative energy calculations. The resolution of identity (RI) approximation[56] was adopted in all calculations. In order to check whether the lowest-energy structures obtained are ground states, simulated PES were generated according to the generalized Koopman's theorem;[57] for an easier comparison with the measured spectra they were broadened by Gaussians of 0.06 eV width.

Other functionals (PBE,[58] BLYP,[50,59] PBE0,[60] M06,[61] M06-2X,[61] B3P[62]) were also tested. It was found that BP86 performs best with respect to reproducing experimental vertical detachment energies (VDEs) and PESs (see Tables S1 and S2 in the ESI†). All structures of the clusters were rendered by the software VMD 1.9.3.[63] Hirshfeld population analysis was performed with Multiwfn 3.8 (dev)[64] using the output of the ORCA program.

Results and discussion

The photoelectron spectra of $TM_2Si_n^-$ (TM = V, n = 14–20; TM = Cr, n = 14–16)

The photoelectron spectra of $V_2Si_{14-20}^-$ and $Cr_2Si_{14-16}^-$ measured with 248 nm photons are shown in Fig. 1. The experimentally measured vertical detachment energies (VDEs) of these cluster anions were evaluated from the maxima of the first peaks of the spectra, and are summarized in Table 1. Several features can be discerned in the spectra labeled by letters X, A, B, C, and D. X represents the transition from the ground state of the anion to that of the neutral, which gives the value of the VDE, whereas A, B, C denote detachment transitions to excited states of the neutral species. X' denotes the presence of a different isomeric structure.

The measured spectrum of $V_2Si_{14}^-$ reveals a very weak X' peak at 2.81 eV, and three clear peaks centered at 3.21, 3.52, and 3.96 eV, followed by a broad band centered above 4.4 eV. In the spectrum of $V_2Si_{15}^-$, there are four peaks centered at 3.59, 3.98, 4.23, and 4.60 eV. Similarly, the spectrum of $V_2Si_{16}^-$ has four peaks centered at 3.83, 4.06, 4.23, and 4.50 eV. The spectrum of $V_2Si_{17}^-$ reveals a ground-state transition X with a VDE of 3.12 eV, a band (A) centered at 4.00 eV, and a broad band B centered at about 4.20 eV, as well as a sharp onset of a band C at 4.50 eV. The band gap between the X and A peaks is about 0.9 eV, indicating a large HOMO–LUMO gap of the corresponding neutral cluster. The spectrum of $V_2Si_{18}^-$ has an almost unresolved peak X at about 3.53 eV, followed by four resolved peaks A, B, C and D centered at 3.68, 3.95, 4.14, and 4.50 eV, respectively. Four bands (X, A, B, and C) can be observed in the spectrum of $V_2Si_{19}^-$, centered at 3.59, 3.88, 3.96, and 4.21 eV, respectively, where the A band consists of two small peaks adjacent to each other. The spectrum of $V_2Si_{20}^-$ is very broad, but three partially resolved peaks (X, A, and B) can still be observed at 3.57, 3.78, and 4.11 eV, followed by a broad band C starting at about 4.3 eV. The spectral features of $V_2Si_{20}^-$ probably indicate a strong vibrational excitation upon photoemission and possibly the presence of several isomers. For $Cr_2Si_n^-$, the measured spectrum of size 14 reveals six clear peaks (X to E), centered at 3.12, 3.35, 3.76, 4.09, 4.28, and 4.51 eV, respectively. For $Cr_2Si_{15}^-$, the first small peak defines a VDE of 3.13 eV, followed by four peaks centered at 3.34, 3.68, 3.92, and 4.34 eV. The spectrum of $Cr_2Si_{16}^-$ has a weak low binding feature X centered at 3.13 eV and three overlapping peaks centered at 3.91, 4.07, and 4.21 eV, followed by a prominent peak centered at 4.44 eV.

In order to obtain the structural and electronic properties of the clusters, geometric structures have been searched globally as described above; the results are shown in Fig. 2. Here for all sizes the three lowest energy isomers are shown together with their calculated relative energies. The PES calculated for these structures are compared to the measured ones in Fig. 1. More structures and the corresponding simulated spectra are displayed in the ESI.† As shown in Fig. 1, the main features of the measured spectra for all V_2 doped clusters can be reproduced by the spectra simulated for the lowest energy structures, except for $V_2Si_{14}^-$ where in fact isomer 14B gives a slightly better fit.

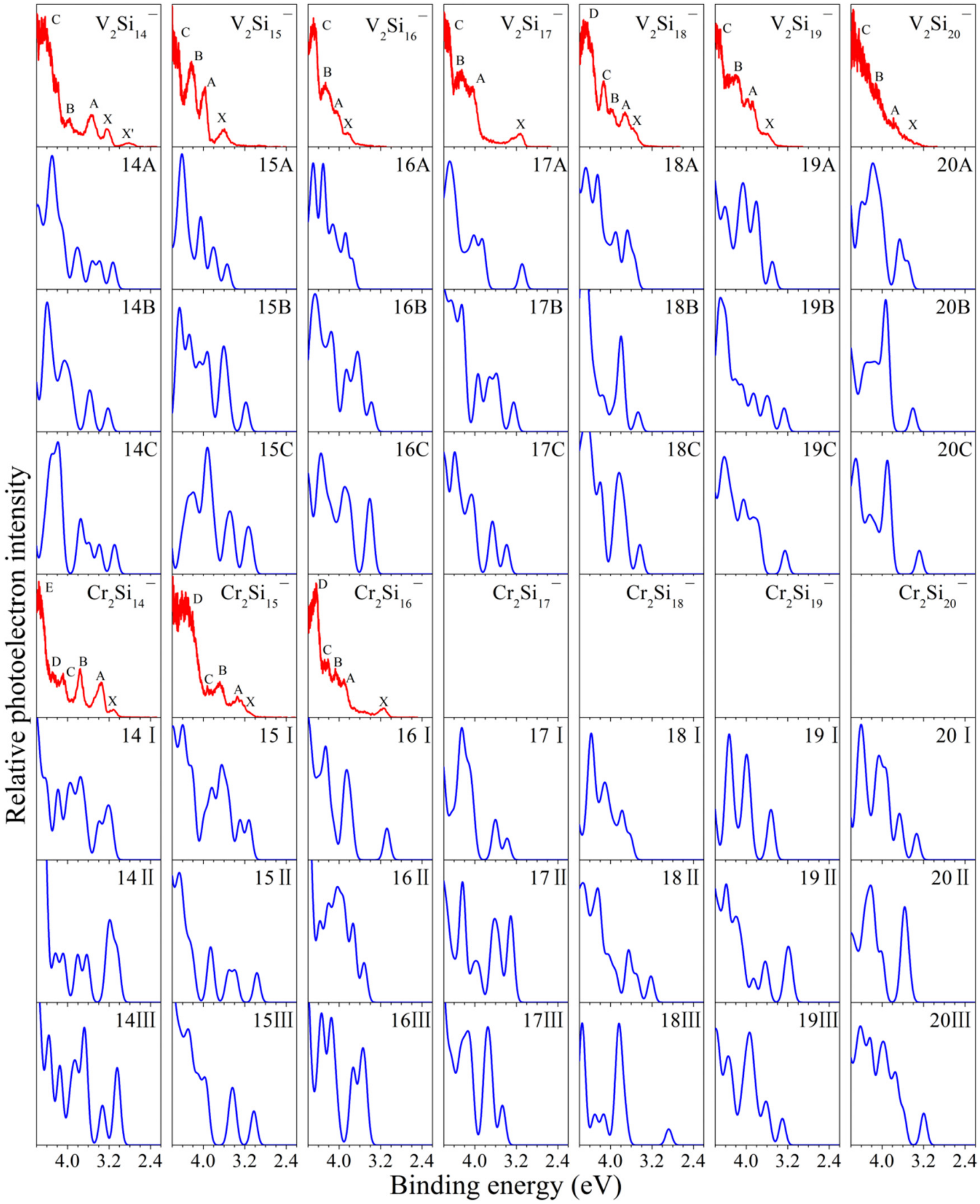

Fig. 1 Experimental (Expt., red lines) photoelectron spectra of $TM_2Si_n^-$ (TM = V, Cr; n = 14–20) clusters, measured at a photon energy of 5.0 eV, and theoretical (Theo., blue lines) electronic density of states, calculated at the BP86/def2-TZVPD level. Three lowest lying isomers are listed as A, B, C and I, II, III for V and Cr doped silicon cluster anions in order of increasing energy, respectively.

Furthermore, for this size unfortunately none of the top three lowest-energy isomers can reproduce the weak peak X' in the experimental spectrum, which is likely to be contributed by a yet unidentified isomer. Isomer 14E shown in Fig. S1 of the ESI,† would in principle have the correct low electron affinity, but is so high in energy that it should not be present in the experiment. For the Cr_2 doped clusters the agreement between measured and simulated PES is less good than in the V_2 case, which might hint at the fact that a different functional should be used for calculating the electronic density of states in this case. Nevertheless, for size n = 16 the assignment is certainly convincing as the lowest energy isomer found is the only one with a bandgap between first and second peak comparable to the large one seen in the experiment. We assume that the global minimum searching scheme was similarly successful also for the other sizes, but certainly more experimental work

Table 1 Spin multiplicity (SM), average Si–Si, TM–Si, and TM–TM bond lengths, binding energies (E_b), HOMO-LUMO gaps (Gap), second order difference in energy (Δ^2E), and theoretical (Theo.) and experimental (Expt.) vertical detachment energies (VDEs) of the lowest-energy structures of $TM_2Si_n^-$ (TM = V, Cr; n = 14–20) clusters. The uncertainties of experimental VDEs are ±0.03 eV. The units of bond length and energy are Å and eV, respectively

		Bond length (Å)						VDEs (eV)	
Cluster	SM	Si–Si	TM–Si	TM–TM	Δ^2E (eV)	E_b (eV)	Gap (eV)	Theo.	Expt.
$V_2Si_{14}^-$	2	2.48	2.65	2.33	—	4.034	0.303	3.13	3.21
$V_2Si_{15}^-$	2	2.49	2.64	2.33	0.025	4.037	0.463	3.54	3.59
$V_2Si_{16}^-$	2	2.47	2.68	2.35	0.289	4.039	0.332	3.74	3.83
$V_2Si_{17}^-$	2	2.49	2.69	2.35	−0.859	4.025	0.541	3.09	3.12
$V_2Si_{18}^-$	2	2.37	2.65	2.46	0.721	4.056	0.262	3.54	3.53
$V_2Si_{19}^-$	2	2.41	2.70	2.73	−0.218	4.049	0.375	3.50	3.59
$V_2Si_{20}^-$	2	2.39	2.70	2.46	—	4.053	0.194	3.50	3.57
$Cr_2Si_{14}^-$	2	2.36	2.65	2.17	—	3.748	0.279	3.16	3.12
$Cr_2Si_{15}^-$	2	2.42	2.68	2.20	−0.021	3.771	0.368	3.12	3.13
$Cr_2Si_{16}^-$	2	2.47	2.65	2.27	0.038	3.793	0.505	3.08	3.13
$Cr_2Si_{17}^-$	2	2.40	2.57	2.32	−0.582	3.810	0.235	3.38	—
$Cr_2Si_{18}^-$	2	2.35	2.66	2.32	1.050	3.855	0.451	3.62	—
$Cr_2Si_{19}^-$	2	2.35	2.66	2.40	−0.346	3.845	0.255	3.50	—
$Cr_2Si_{20}^-$	2	2.40	2.69	2.55	—	3.853	0.216	3.34	—

and better simulations are necessary to fully corroborate that the structures identified here are the true ground state structures.

Structures of the $TM_2Si_n^-$ (TM = V,Cr; n = 14–20)

All structures found belong to two structural families. The smaller clusters exhibit structures based on a silicon hexagonal prism or antiprism surrounding a TM dimer, capped by further silicon atoms. The stability of such hexagonal arrangements has been known for a long time; the hexagonal prism variant has for example been predicted for neutral $CrSi_{12}$ clusters by Khanna *et al.* already in 2002[20] and for VSi_{12} anions by Huang *et al.* in 2014.[12] Hexagonal antiprisms have already been found for example for $V_2Si_{12}^-$,[12] Cr_2Si_{13}, $Cr_3Si_{12}^{0/-}$ [46] and $Mn_2Si_{12,13}$.[65]

Larger clusters (with $n \geq 18$ for V and $n \geq 17$ for Cr) instead adopt structures which are more fullerene-like. In these structures the TM atoms can be seen as being individually surrounded by cages of slightly different structure; one of them (always the lower one in Fig. 2) is surrounded by a cage consisting of 12 silicon atoms and the other TM atom, which has a geometry close to that of the fullerene-like isomer of $CrSi_{14}$;[30,66] it can be generated from this fullerene-like isomer by removement of one Si atom and slight rearrangement of the other atoms (Fig. 3). The other TM atom is surrounded by a more densely packed cage, except for $Cr_2Si_{19}^-$, where both Cr atoms are surrounded by the same fullerene-like cage. Also $V_2Si_{18}^-$ is somewhat special, as here the fullerene-like cage around the lower V atom is oriented differently than in all the other cases.

In more detail, for $V_2Si_{14}^-$, all three lowest-lying isomers 14A, 14B and 14C adopt a structure with a V_2 surrounded by a hexagonal antiprism Si_{12}, and capped by two extra silicon atoms at different positions. The lowest-energy isomer of $V_2Si_{15}^-$ (15A) is obtained from $V_2Si_{14}^-$ (14A) by adding a Si on the top. Isomer 15B has a total energy 0.290 eV higher than 15A, and adopts a distorted $V_2@Si_{12}$ hexagonal prism as structural motif with three extra Si atoms added on top. The isomer 15C lies 0.387 eV higher in energy than 15A and adopts a fullerene-like Si_{14} cage structure with an enclosed V atom and a V atom added to a pentagonal facet as well as a Si atom added on top. For $V_2Si_{16}^-$ the lowest-lying structure is almost that of $V_2Si_{15}^-$ cluster with a Si atom added on top except that the hexagonal antiprism is rotated 30 degrees. The isomer 16B can be obtained by adding a Si atom to the three Si atoms on top of isomer 15B. 16C can be seen as a deformed 15B with an extra silicon atom added to the bottom. Isomers 17A and 17B can be constructed by adding an additional Si atom to isomers 16A and 16B, respectively. Isomer 17C can be seen as isomer 14A with a triangle of Si atoms added on top. For sizes $n \geq 18$, both V atoms can be considered as fully embedded in the cage. As mentioned before, the putative ground state structure of $V_2Si_{18}^-$ is special, with the lower V atom embedded in a fullerene-like cage (as present in 15C as well), while the upper V atom can be seen as enclosed within a pentagonal prism. The structure of 18B is a hexagonal prism (D_{2h}), while 18C is composed of a distorted hexagonal prism around the lower and a distorted pentagonal prism around the upper V atom. 19A can be seen as the modified fullerene-like cage structure from Fig. 3 with a ring of seven Si atoms added on top of the upper V atom. The structures of 19B and 19C can be formed by adding a Si atom to 18A and 18C, respectively. Structure 20A is 19A with an atom added to the seven-membered ring, accompanied by a deformation of the latter. Isomer 20B, a distorted Si dodecahedron around a V_2 dimer, was reported by Xu *et al.* as the ground-state structure of this size.[13] In our calculation it has a total energy 0.046 eV higher than 20A, which means that it is probably not the ground state, but might well be present in the experiment. The rather featureless photoelectron spectrum of this size indeed indicates that more than one isomer could contribute to it. Isomer 20C finally has a rather irregular structure.

The structures of the Cr_2-doped Si clusters identified in the calculations are similar to those of the $V_2Si_n^-$ clusters. Both isomers of $Cr_2Si_{14}^-$ 14I and 14III adopt the distorted Si_{12} hexagonal prism as the structural motif, with one Cr atom inside, one Cr atom exposed, and two Si atoms on top. 14II has the hexagonal antiprism structure with a relative energy of 0.021 eV to isomer 14I. For $Cr_2Si_{15}^-$, the isomers 15I and 15II share the same configurations as isomers 15B and 15A of $V_2Si_{15}^-$. Isomer 15III can be obtained by moving a Si atom from the bottom of 15II to the top. The putative ground state of $Cr_2Si_{16}^-$ adopts the same configuration as that of $V_2Si_{16}^-$. Isomer 16II can be seen as two partially merged distorted pentagonal prisms surrounding each of the Cr atoms. Isomer 16III has a tube-like structure consisting of two five-membered and one six-membered ring of Si atoms, with the two Cr atoms embedded inside. Starting from size 17, the putative lowest-energy structures of $Cr_2Si_n^-$ clusters are again based on the modified fullerene structure (Fig. 3). For isomer 17I, this structure is topped by a five-membered ring of Si atoms. Isomers 17II and 17III can be regarded as extensions of 15I

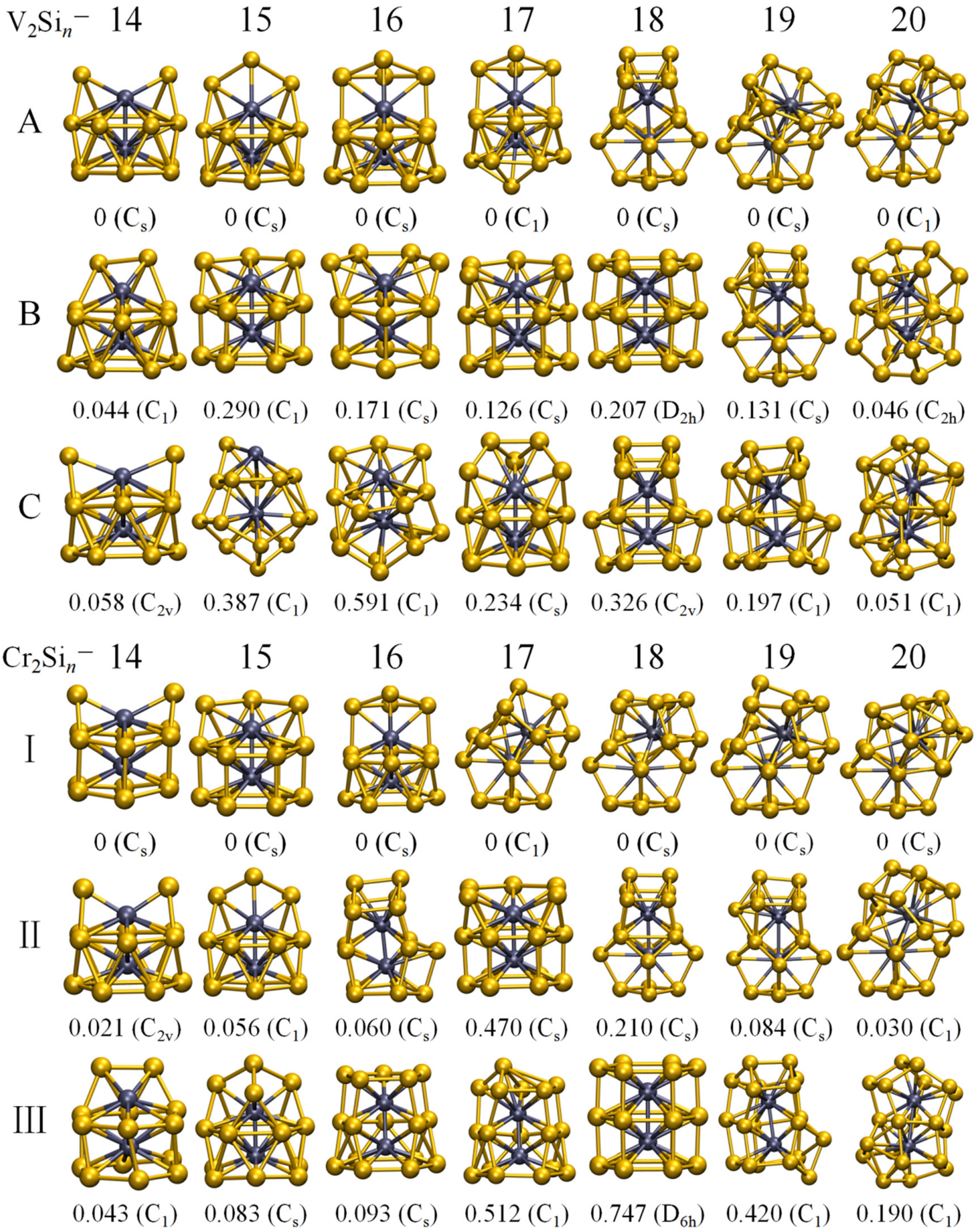

Fig. 2 Lowest-lying isomers of $TM_2Si_n^-$ (TM = V, Cr; n = 14–20). For each size, the total energy difference (eV) with respect to the lowest-energy isomer is provided and the symmetry is given inside brackets. Grey and yellow balls represent TM and Si atoms, respectively.

and 16III, respectively. The lowest energy state found for $Cr_2Si_{18}^-$ consists of the fullerene-like structure topped by six atoms, which almost form a second fullerene-like cage. Isomers 18II and 18III are similar to 18A and 18B of $V_2Si_{18}^-$. As mentioned above, the structure identified for $Cr_2Si_{19}^-$ consists of two merged fullerene-like cage structures – it can be generated from 18I by adding an extra Si atom. Isomers 19II and 19III adopt the same configurations as isomers 19B and 19C of $V_2Si_{19}^-$. Isomer 20I is again based on the fullerene-like structure, now with eight Si atoms added, and can be generated from isomer 19I by shifting one Si atom and adding another one. Isomers 20II and 20III adopt the same configurations as 20A and 20C of $V_2Si_{20}^-$, respectively.

Average Si–Si, TM–Si, and TM–TM bond lengths for the ground-state structures are shown in Fig. 4 and displayed in Table 1. One can observe that the changes of the average TM–Si

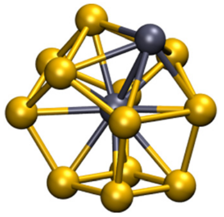

Fig. 3 The partial structural motif TM_2Si_{12} present in all $V_2Si_n^-$ clusters with $n \geq 18$ and $Cr_2Si_n^-$ with $n \geq 17$ (here taken from $V_2Si_{19}^-$, by removing the upper seven-membered ring of Si atoms). It can be generated from a fullerene-like TM@Si_{14} structure[30,65] by removing one of the Si atoms and replacing another one by a TM atom. In the case of $V_2Si_{18}^-$ the Si atom and the TM atom on top of the cage are exchanged.

and Si–Si bond lengths change are not as obvious as that for TM–TM bond in this size range. The average Si–Si bond length in $V_2Si_{18}^-$ is shorter than that in neighboring sizes, which is mainly due to higher symmetry structure of the cluster. In the ESI,† in Fig. S8 the bond length distributions are shown; one can see that in $V_2Si_{18}^-$ the distribution is much narrower than for the other sizes. This more uniform structure and the shorter bond length is also reflected in a slightly higher average Wilberg bond order of the Si-Si bonds, compared to that of the neighboring sizes (Fig. 5).

The Si–Si bond length in $V_2Si_{14}^-$ ($V_2Si_{15}^-$) is larger than that in Cr_2Si_{14} ($Cr_2Si_{15}^-$), mainly due to the fact that in the former case an hexagonal antiprism is formed, which has slightly larger Si–Si distances than those in the hexagonal prism formed in the latter case. The preference for the different types of prism structures probably stems from the longer TM–TM bond lengths in the vanadium case. Again the longer bond Si–Si bond lengths are reflected in the respective Wilberg bond orders (Fig. 5). In contrast the TM–TM bond lengths exhibit a significant size dependence, which is obviously due to a weakening of the TM–TM bond with increasing coordination of the TM atoms. Interestingly the Cr–Cr bond exhibits a stronger increase with size than the V–V bond. One exception is $V_2Si_{19}^-$; here the especially high coordination of one of the V atoms by a seven-membered ring of Si atom seems to cause an enhanced weakening of the V–V bond.

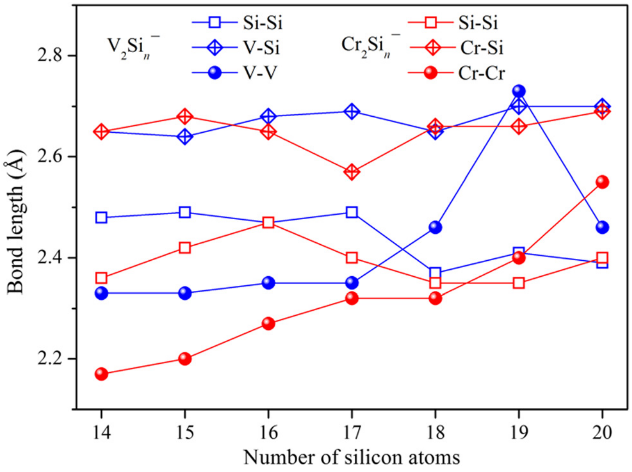

Fig. 4 TM–TM bond length and average Si–Si and TM–Si bond lengths of the lowest-lying isomers of $TM_2Si_n^-$ (TM = V, Cr; n = 14–20).

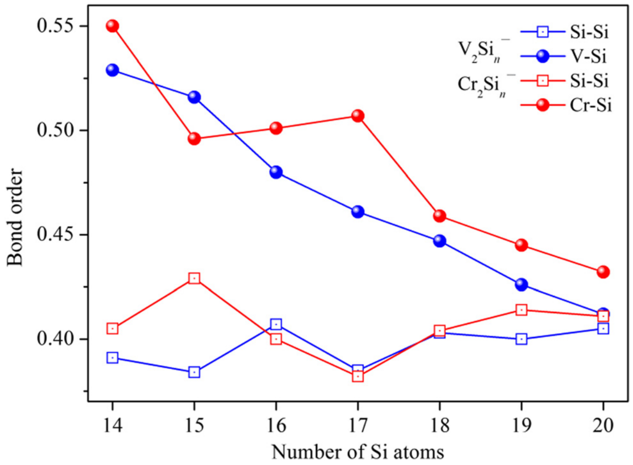

Fig. 5 Wiberg bond orders (BO) of Si–Si and TM–Si bonds for the ground state structures of $TM_2Si_n^-$ (TM = V, Cr; n = 14–20) clusters as a function of the number of Si atoms.

Overall the TM-TM bonds are much larger than the corresponding gas phase dimer bond lengths (V_2: 1.77 Å;[67] Cr_2: 1.68 Å[68]), but for the smallest clusters still smaller than the nearest neighbor distances in bulk (V: 2.62 Å;[69] Cr: 2.52 Å[70]). For the largest size they are close to or (in the case of Cr) larger than the bulk values; it would be interesting to see how this develops for even larger sizes.

Electronic properties of $TM_2Si_n^-$ (TM = V, Cr; n = 14–20) clusters

A number of cluster properties are summarized and compared to experimental values in Table 1 and shown in Fig. 6. Fig. 6(a) shows the experimental and theoretical VDEs of the clusters as a function of the number of silicon atoms. The measured VDEs for V_2Sin^- increase with n from 14 to 16 and abruptly drop to 3.09 eV at n = 17, gradually rising up again from n = 18 to 20. The theoretical VDEs reproduce this trend well, with a little underestimation of the VDEs by 0.09 eV and 0.07 eV for $V_2Si_{19}^-$ and $V_2Si_{20}^-$, respectively. This, in addition to the qualitative agreement between the experimental spectra and the theoretical simulations discussed above, provides evidence that the correct structures of $V_2Si_n^-$ (n = 14–20) clusters have indeed been found. The VDEs of $Cr_2Si_n^-$ clusters remain nearly constant in the size range of n = 14–16, but exhibit larger values for the larger sizes, which might reflect the structural transition taking place between n = 16 and 17. To investigate the stability of the clusters, we calculated the average binding energy as defined by $E_b(TM_2Si_n^-) = [(n-1)E(Si) + E(Si^-) + 2E(TM) - E(TM_2Si_n^-)]/(n+2)$, where $E(TM_2Si_n^-)$ represents the energy of the anionic $TM_2Si_n^-$ cluster, E(Si), E(TM) and $E(Si^-)$ are the energies of a Si atom, TM atom and Si anion, respectively. The corresponding results are presented as a function of the number of silicon atoms in Fig. 6(b). For both clusters the binding energy increases

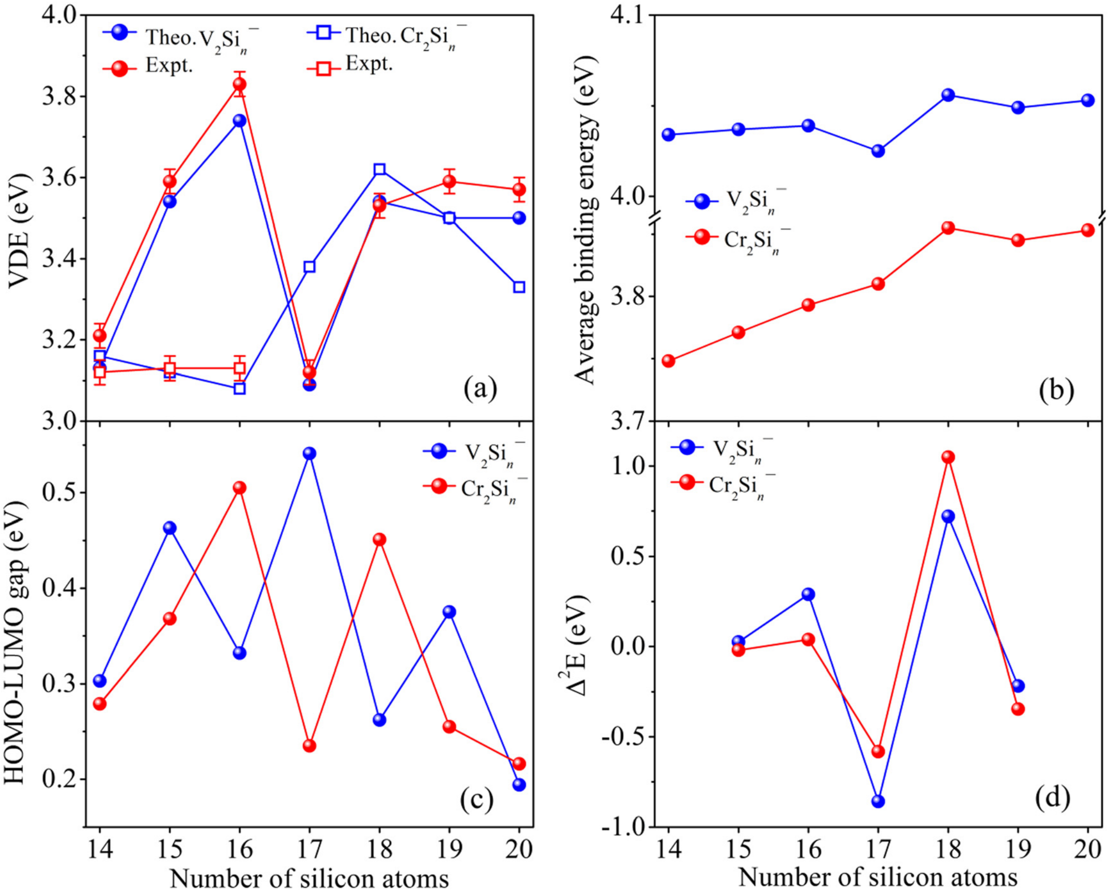

Fig. 6 (a) Experimental and theoretical VDEs of $TM_2Si_n^-$ (TM = V, Cr; n = 14–20) cluster anions shown as a function of cluster size. The red spheres and open squares are experimental values with an uncertainty of 0.03 eV; the blue spheres and open triangles represent the theoretical values from the lowest-energy structures found. The average binding energies (b), HOMO–LUMO gaps (c) and the second order differences in energy $\Delta_2E(n) = E(n-1) + E(n+1) - 2E(n)$ (d) of the lowest energy structures are plotted against the number of silicon atoms.

with size; interestingly the slope is significantly higher for the Cr_2 doped clusters. As the Cr_2 doped clusters also exhibit the stronger increase of the TM–TM bond lengths with size, one could speculate that the stronger weakening of the TM–TM bond is accompanied by an enhanced strengthening of the TM–Si bonds. For both dopants one can observe deviations from a smooth increase at sizes 17 and 18. This is even better seen in Fig. 6(d), where the second order differences of the cluster total energies $\Delta_2E(n) = E(n-1) + E(n+1) - 2 \times E(n)$ are shown. For both dopants size 17 exhibits a lower stability, while size 18 exhibits strongly enhanced stability. Due to the different electron count in these systems this should be a geometric effect, which is somewhat surprising as they do not share the same structures. One could speculate that 18 is just the ideal number of Si atoms for a cage enclosing the TM dimers, despite their slightly different sizes.

Finally, we calculated the HOMO–LUMO gaps of the clusters, which are presented in Fig. 6(c). The values exhibit prominent even–odd alternations, with reversed maxima and minima for the two dopants. From the results of HOMO–LUMO gaps of other isomers of $TM_2Si_n^-$(TM = V, Cr; n = 14–20) in Fig. S7 in ESI,† the even-odd oscillation of HOMO–LUMO gaps of the ground state structures of $V_2Si_n^-$ cluster should be a coincidence, caused by the interaction of electronic and geometric structures. Taking $V_2Si_{17}^-$ as an example, the HOMO–LUMO gap of 17A is significantly larger than that of 16A or 18A, while those of 17B and 17C are smaller than both of them, showing the significant effect of structure on electronic properties.

A special case, however, are the clusters $Cr_2Si_{16}^-$ and $V_2Si_{17}^-$. Both exhibit a large gap between the X and the A peak in their photoelectron spectra, indicating a large band gap of the corresponding neutral cluster, as well as a large HOMO–LUMO gap. This gives evidence that they might have similar electronic structures. This could well be, as they have almost identical geometrical structures; $V_2Si_{17}^-$ has exactly the geometry of $Cr_2Si_{16}^-$, just with one Si atom added from below. In order to check this we have calculated the orbitals for the uppermost occupied and lowermost unoccupied states for both clusters; these are displayed in Fig. 7.

One can observe that indeed the orbitals of the HOMO and the LUMO as well as of neighboring states are close to identical. This shows that these clusters are indeed isoelectronic, meaning that while, as expected, the Cr dimer adds two more electrons to the system than the V dimer, the additional Si atom also adds two electrons to it and not four as one might naively expect. This indicates that two of the four valence electrons of the added Si atom get localized in form of a lone pair.

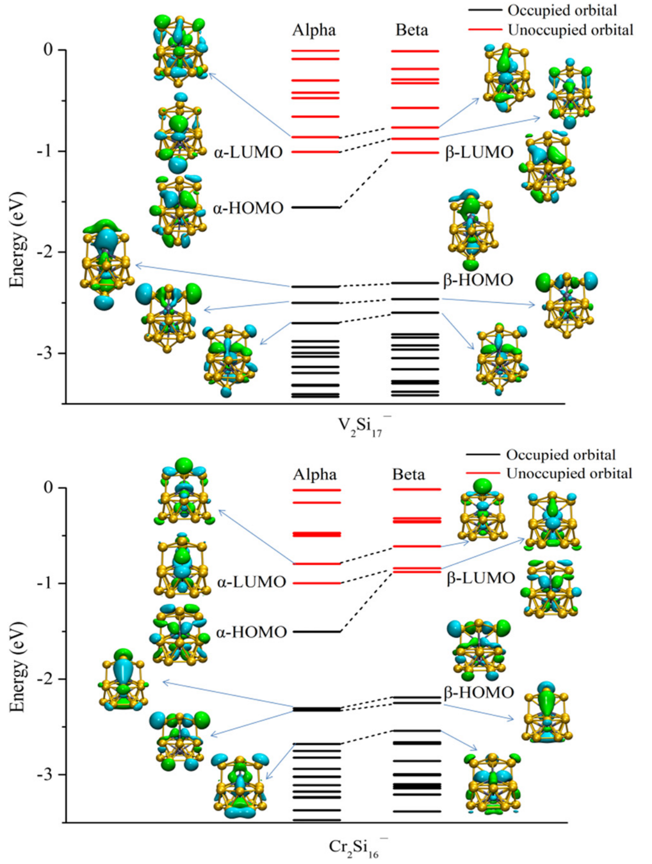

Fig. 7 Calculated energies and orbital of Kohn-Sham levels in $V_2Si_{17}^-$ (upper panel) and $Cr_2Si_{16}^-$ (lower panel) clusters for the two spin directions. The similarity of the orbitals indicate that the clusters are practically isoelectronic.

Table 2 On-site spin moment on the top TM atom and bottom TM atom in $TM_2Si_n^-$ (TM = V, Cr; n = 14–20) cluster anions from Hirshfeld population analysis, along with the total magnetic moment (μ_T). $\mu_{TM\text{-top}}$, $\mu_{TM\text{-bottom}}$ and $\mu_{TM\text{-T}}$ denote the magnetic moments of the upper TM atom, the lower TM atom, and the sum of the two

Clusters	Magnetic moment (μ_B)			
	μ_T	$\mu_{TM\text{-top}}$	$\mu_{TM\text{-bottom}}$	$\mu_{TM\text{-T}}$
$V_2Si_{14}^-$	1	0.257	0.039	0.296
$V_2Si_{15}^-$	1	0.287	0.160	0.447
$V_2Si_{16}^-$	1	0.109	0.324	0.433
$V_2Si_{17}^-$	1	0.688	−0.068	0.620
$V_2Si_{18}^-$	1	0.051	0.203	0.254
$V_2Si_{19}^-$	1	−0.027	0.573	0.546
$V_2Si_{20}^-$	1	0.085	0.018	0.103
$Cr_2Si_{14}^-$	1	0.425	−0.006	0.419
$Cr_2Si_{15}^-$	1	1.191	−0.486	0.705
$Cr_2Si_{16}^-$	1	0.780	0.177	0.957
$Cr_2Si_{17}^-$	1	0.024	−0.001	0.023
$Cr_2Si_{18}^-$	1	1.006	−0.626	0.380
$Cr_2Si_{19}^-$	1	0.532	−0.241	0.291
$Cr_2Si_{20}^-$	1	0.228	0.094	0.322

Magnetic properties of $TM_2Si_n^-$ (TM = V, Cr; n = 14–20) clusters

In order to gain insight into the magnetic properties of the clusters, spin electron density isosurface calculations and Hirshfeld population analysis were conducted, the results of which are displayed in Fig. 8 and summarized in Table 2. All results presented here were obtained at the BP86/def2-TZVPD level. Results for different functionals are given in ESI,† Tables S3 and S4. It turns out that the results for the three functionals BP86, PBE and BLYP are very similar, while rather different results are obtained for the hybrid functionals PBE0 and B3P. The addition of exact exchange leads to stronger local moments and an even stronger tendency towards the antiferromagnetic order discussed below. As the functional BP86 gave the best agreement with the experimental results in terms of the VDE and the electronic density of states, we here discuss just the results obtained with this functional in more detail. Nevertheless we want to stress that the results do depend on the type of functional used.

As shown in Fig. 8, in $V_2Si_{14}^-$, the excess alpha electrons, marked by the green zones, appear around the upper V atom, which contributes $0.257\mu_B$ to the total spin magnetic moment.

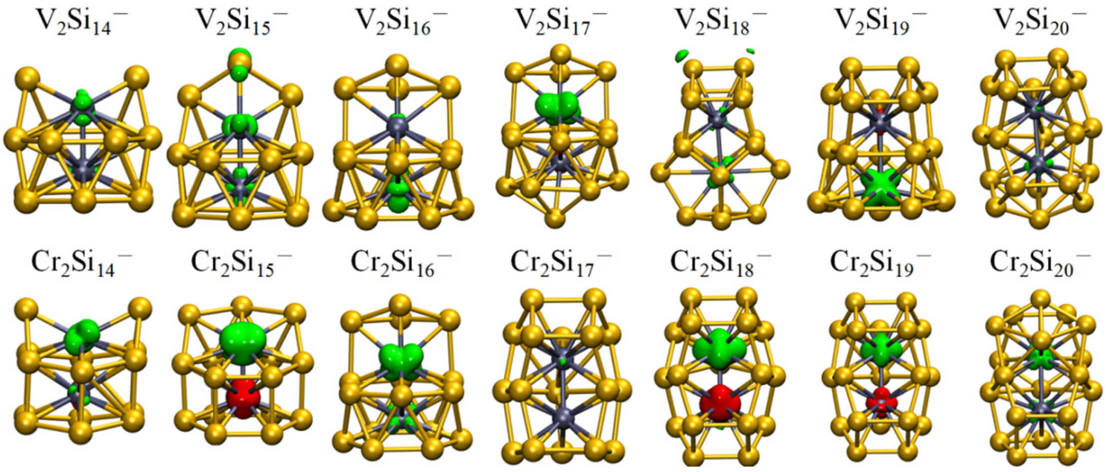

Fig. 8 Isosurface maps of the electron spin density of the lowest-energy $TM_2Si_n^-$ (TM = V, Cr; n = 14–20) clusters. The isosurface is set to ±0.01 e Å^{-3}. Green and red isosurfaces indicate the positive and negative electron spin density, respectively.

For $V_2Si_{15}^-$, they appear around the two V atoms and the vertex Si atom. Interestingly, the contribution of the atom at the vertex is $0.326\mu_B$, which is greater than those of the two V atoms ($0.287\mu_B$ and $0.160\mu_B$, respectively). The excess alpha electrons also appear around the two V atoms in $V_2Si_{16}^-$, where the enclosed (the bottom one) V atom contributes the most ($0.324\mu_B$). $V_2Si_{17}^-$ can be seen as a $V_2Si_{16}^-$ with a Si atom added to the bottom, but still there is a significant change of the spin electron density, where the excess alpha electrons are now concentrated around the top V atom, which contributes $0.688\mu_B$ to the total spin magnetic moment. Regarding $V_2Si_{18}^-$, the bottom V atom contributes the most ($0.203\mu_B$) followed by the two Si atoms on the top, which contribute $0.181\mu_B$ and $0.163\mu_B$, respectively, while the contribution of the top V atom is minute ($0.051\mu_B$). For $V_2Si_{19}^-$, the alpha electrons mainly concentrate around the V atom at the bottom. In the case of $V_2Si_{20}^-$, the total magnetic moment is mainly contributed by the Si cage.

Although most of $V_2Si_n^-$ and $Cr_2Si_n^-$ clusters (n = 14–20) share similar structures and the exact same total spin magnetic moment, the magnetic constitutions are very distinct. For $Cr_2Si_{14}^-$, the top Cr atom contributes the largest magnetic moment of $0.425\mu_B$. For $Cr_2Si_{15}^-$, the excess alpha and beta electrons appear around the top and bottom Cr atoms. The spin population analysis shows that the top and bottom Cr atoms contribute $1.191\mu_B$ and $-0.486\mu_B$, respectively. Similar to $Cr_2Si_{14}^-$, the excess alpha electrons also appear around the top Cr atom in $Cr_2Si_{16}^-$. Interestingly, for $Cr_2Si_{17}^-$ the spins are evenly distributed, and the two Cr atoms contribute very little. Similar to $Cr_2Si_{15}^-$, in $Cr_2Si_{18}^-$ and $Cr_2Si_{19}^-$, the two Cr atoms contribute opposite magnetic moments. In $Cr_2Si_{20}^-$, the top and bottom Cr atoms contribute $0.228\mu_B$ and $0.094\mu_B$ to the total magnetic moments, respectively.

Conclusions

In summary, the structural evolution and electronic properties of $TM_2Si_n^-$ (TM = V, Cr; n = 14–20) clusters were investigated by using anion PES and DFT calculations. Putative ground-state structures of the clusters have been identified. The two TM atoms prefer to stay together and form a TM–TM bond shorter than the nearest neighbor distance in the metallic bulk, except for $V_2Si_{19}^-$ cluster where the V–V bond is longer than in the bulk. Two structural families have been identified; while the smaller sizes are based on silicon hexagonal prisms or antiprisms surrounding one of the TM atoms, the larger ones exhibit more fullerene-like structures. Here one of the TM atoms is surrounded by a cage formed by 12 Si atoms and the other TM atom, which strongly resembles the fullerene-like cage present in $TMSi_{14}$ (TM = V, Cr) clusters. The transition between the two structural motifs occurs at n = 18 for V and n = 17 for Cr doped clusters. Photoelectron spectra and electronic structure calculations reveal that $Cr_2Si_{16}^-$ and $V_2Si_{17}^-$ clusters can be seen as isoelectronic. $TM_2Si_{18}^-$ clusters turn out to be most stable for both dopants. All clusters are predicted to be in the lowest possible spin state (doublet), but with very different contributions from the dopants. In $Cr_2Si_{15,18,19}^-$ clusters, according to the calculations the two Cr atoms contribute opposite magnetic moments, thus showing an antiferromagnetic state.

Conflicts of interest

The authors declare no competing financial interest.

Acknowledgements

This work was supported by the National Natural Science Foundation of China under Grant No. 11774255, the National Key R&D Program of China No. 2020YFC2004602.

References

1 S. M. Beck, *J. Chem. Phys.*, 1987, **87**, 4233–4234.
2 S. M. Beck, *J. Chem. Phys.*, 1989, **90**, 6306–6312.
3 M. Ohara, K. Koyasu, A. Nakajima and K. Kaya, *Chem. Phys. Lett.*, 2003, **371**, 490–497.
4 K. Koyasu, M. Akutsu, M. Mitsui and A. Nakajima, *J. Am. Chem. Soc.*, 2005, **127**, 4998–4999.
5 S. Neukermans, X. Wang, N. Veldeman, E. Janssens, R. E. Silverans and P. Lievens, *Int. J. Mass Spectrom.*, 2006, **252**, 145–150.
6 S.-J. Lu, H.-G. Xu, X.-L. Xu and W.-J. Zheng, *J. Phys. Chem. A*, 2020, **124**, 9818–9831.
7 S. Furuse, K. Koyasu, J. Atobe and A. Nakajima, *J. Chem. Phys.*, 2008, **129**, 064311.
8 H.-G. Xu, Z.-G. Zhang, Y. Feng, J. Yuan, Y. Zhao and W. Zheng, *Chem. Phys. Lett.*, 2010, **487**, 204–208.
9 X. Wu, Q. Du, S. Zhou, X. Huang, M. Chen, L. Miao, G. Yin, J. Wang, K. Wang, B. V. Issendorff, L. Ma and J. Zhao, *Eur. Phys. J. Plus*, 2020, **135**, 734.
10 H.-G. Xu, M. M. Wu, Z.-G. Zhang, J. Yuan, Q. Sun and W. Zheng, *J. Chem. Phys.*, 2012, **136**, 104308.
11 A. Nakajima, *Bull. Chem. Soc. Jpn.*, 2013, **86**, 414–437.
12 X. Huang, H.-G. Xu, S. Lu, Y. Su, R. B. King, J. Zhao and W. Zheng, *Nanoscale*, 2014, **6**, 14617–14621.
13 H.-G. Xu, X.-Y. Kong, X.-J. Deng, Z.-G. Zhang and W.-J. Zheng, *J. Chem. Phys.*, 2014, **140**, 024308.
14 S.-J. Lu, G.-J. Cao, X.-L. Xu, H.-G. Xu and W.-J. Zheng, *Nanoscale*, 2016, **8**, 19769–19778.
15 S.-J. Lu, X.-L. Xu, H.-G. Xu and W.-J. Zheng, *J. Chem. Phys.*, 2018, **148**, 244306.
16 W.-S. Dai, B. Yang, S.-T. Yan, H.-G. Xu, X.-L. Xu and W.-J. Zheng, *J. Phys. Chem. A*, 2021, **125**, 10557–10567.
17 B. Yang, X.-L. Xu, H.-G. Xu, U. Farooq and W.-J. Zheng, *Phys. Chem. Chem. Phys.*, 2019, **21**, 6207–6215.
18 K. Wang, H.-Y. Zhao, L. Miao, Z.-Z. Jia, G.-J. Yin, X.-D. Zhu, R. Moro, B. V. Issendorff and L. Ma, *J. Phys. Chem. A*, 2022, **126**, 1329–1335.
19 V. Kumar and Y. Kawazoe, *Phys. Rev. Lett.*, 2001, **87**, 045503.

20 S. N. Khanna, B. K. Rao and P. Jena, *Phys. Rev. Lett.*, 2002, **89**, 016803.

21 V. Kumar, T. M. Briere and Y. Kawazoe, *Phys. Rev. B: Condens. Matter Mater. Phys.*, 2003, **68**, 155412.

22 V. Kumar and Y. Kawazoe, *Phys. Rev. B: Condens. Matter Mater. Phys.*, 2002, **65**, 073404.

23 P. Guo, Z.-Y. Ren, F. Wang, J. Bian, J.-G. Han and G.-H. Wang, *J. Chem. Phys.*, 2004, **121**, 12265–12275.

24 J. Ulises Reveles and S. N. Khanna, *Phys. Rev. B: Condens. Matter Mater. Phys.*, 2005, **72**, 165413.

25 N. Uchida, T. Miyazaki and T. Kanayama, *Phys. Rev. B: Condens. Matter Mater. Phys.*, 2006, **74**, 205427.

26 J. U. Reveles and S. N. Khanna, *Phys. Rev. B: Condens. Matter Mater. Phys.*, 2006, **74**, 035435.

27 L.-J. Guo, X. Liu, G.-F. Zhao and Y.-H. Luo, *J. Chem. Phys.*, 2007, **126**, 234704.

28 M. B. Torres, E. M. Fernández and L. C. Balbás, *Phys. Rev. B: Condens. Matter Mater. Phys.*, 2007, **75**, 205425.

29 J. Wang and J. H. Liu, *J. Phys. Chem. A*, 2008, **112**, 4562–4567.

30 J. He, K. Wu, C. Liu and R. Sa, *Chem. Phys. Lett.*, 2009, **483**, 30–34.

31 W. Ji and C. Luo, *Int. J. Quantum Chem.*, 2011, **112**, 2525–2531.

32 H. Kawamura, V. Kumar and Y. Kawazoe, *Phys. Rev. B: Condens. Matter Mater. Phys.*, 2004, **70**, 245433.

33 M. B. Abreu, A. C. Reber and S. N. Khanna, *J. Phys. Chem. Lett.*, 2014, **5**, 3492–3496.

34 D. Kim, D. U. Lee, E. K. Kim, S.-W. Lee, S.-M. Jung and W.-J. Cho, *J. Alloys Compd.*, 2013, **559**, 1–4.

35 R. K. Waits, *Thin Solid Films*, 1973, **16**, 237–247.

36 M. Jhabvala, R. S. Babu, C. Monroy, M. M. Freund and C. D. Dowell, *Cryogenics*, 2002, **42**, 517–526.

37 D. Caputo, G. de Cesare, A. Nascetti and M. Tucci, *Thin Solid Films*, 2007, **515**, 7517–7521.

38 S. Zhou, X. Yang, W. Pei, J. Zhao and A. Du, *J. Phys. Chem. C*, 2019, **123**, 9973–9980.

39 R. Robles, S. N. Khanna and A. W. Castleman, *Phys. Rev. B: Condens. Matter Mater. Phys.*, 2008, **77**, 235441.

40 P. Claes, E. Janssens, V. T. Ngan, P. Gruene, J. T. Lyon, D. J. Harding, A. Fielicke, M. T. Nguyen and P. Lievens, *Phys. Rev. Lett.*, 2011, **107**, 173401.

41 K. Koyasu, J. Atobe, S. Furuse and A. Nakajima, *J. Chem. Phys.*, 2008, **129**, 214301.

42 W. Zheng, J. M. Nilles, D. Radisic and K. H. Bowen, *J. Chem. Phys.*, 2005, **122**, 071101.

43 X. Kong, H.-G. Xu and W. Zheng, *J. Chem. Phys.*, 2012, **137**, 064307.

44 K. Koyasu, J. Atobe, M. Akutsu, M. Mitsui and A. Nakajima, *J. Phys. Chem. A*, 2007, **111**, 42–49.

45 X. Huang, S.-J. Lu, X. Liang, Y. Su, L. Sai, Z.-G. Zhang, J. Zhao, H.-G. Xu and W. Zheng, *J. Phys. Chem. C*, 2015, **119**, 10987–10994.

46 B. Yang, H. Xu, X. Xu and W. Zheng, *J. Phys. Chem. A*, 2018, **122**, 9886.

47 L. Ma, B. v Issendorff and A. Aguado, *J. Chem. Phys.*, 2010, **132**, 104303.

48 X. W. Wu, X. Liang, Q. Du, J. Zhao, M. Chen, L. Miao, J. Wang, G. Yin, L. Ma, R. B. King and B. V. Issendorff, *J. Phys.: Condens. Matter*, 2018, **30**, 354002.

49 J. P. Perdew, *Phys. Rev. B: Condens. Matter Mater. Phys.*, 1986, **33**, 8822–8824.

50 A. D. Becke, *Phys. Rev. A: At., Mol., Opt. Phys.*, 1988, **38**, 3098–3100.

51 F. Weigend and R. Ahlrichs, *Phys. Chem. Chem. Phys.*, 2005, **7**, 3297.

52 F. Weigend, *Phys. Chem. Chem. Phys.*, 2006, **8**, 1057–1065.

53 F. Neese, *Wiley Interdiscip. Rev.: Comput. Mol. Sci.*, 2012, **2**, 73–78.

54 F. Neese, *Wiley Interdiscip. Rev.: Comput. Mol. Sci.*, 2017, **8**, e1327.

55 D. Rappoport and F. Furche, *J. Chem. Phys.*, 2010, **133**, 134105.

56 F. J. Neese, *Comput. Chem.*, 2003, **24**, 1740–1747.

57 J. Akola, M. Manninen, H. Häkkinen, U. Landman, X. Li and L.-S. Wang, *Phys. Rev. B: Condens. Matter Mater. Phys.*, 1999, **60**, R11297–R11300.

58 J. P. Perdew, K. Burke and M. Ernzerhof, *Phys. Rev. Lett.*, 1996, **77**, 3865–3868.

59 C. Lee, W. Yang and R. G. Parr, *Phys. Rev. B: Condens. Matter Mater. Phys.*, 1988, **37**, 785–789.

60 C. Adamo, *J. Chem. Phys.*, 1999, **110**, 6158–6170.

61 Y. Zhao and D. Truhlar, *Theor. Chem. Acc.*, 2008, **120**, 215–241.

62 A. D. Becke, *J. Chem. Phys.*, 1993, **98**, 5648–5652.

63 W. Humphrey, A. Dalke and K. Schulten, *J. Mol. Graphics*, 1996, **14**(1), 33–38.

64 T. Lu and F. Chen, *J. Comput. Chem.*, 2012, **33**(5), 580–592.

65 V. Khanna, R. Singh, P. Claes, M. T. Nguyen, A. Fielicke, E. Janssens, P. Lievens and J. E. McGrady, *J. Phys. Chem. A*, 2022, **126**, 1617–1626.

66 X. Jin, V. Arcisauskaite and J. E. McGrady, *Dalton Trans.*, 2017, **46**, 11636–11644.

67 P. R. R. Langridge-Smith, M. D. Morse, G. P. Hansen, R. E. Smalley and A. J. Merer, *J. Chem. Phys.*, 1984, **80**, 593.

68 D. L. Mlchalopoulos, E. Geusic, S. G. Hansen, D. E. Powers and R. E. Smalley, *J. Phys. Chem.*, 1982, **86**, 3914–3916.

69 R. W. G. Wyckoff, *Crystal Structures*, Interscience, New York, 2nd edn, 1963.

70 A. W. Hull, *Phys. Rev.*, 1921, **17**, 571–588.